An assessment of vortex detection criteria for 2C-2D PIV data

An assessment of vortex detection criteria for 2C-2D PIV data

An assessment of vortex detection criteria for 2C-2D PIV data

F De Gregorio[1*], A Visingardi[2], M Coletta[3], G Iuso[3]

[1]Italian Aerospace Research Centre, Aerodynamic and Icing Measurement, Capua, Italy
[2]Italian Aerospace Research Centre, Fluid Mechanics, Capua, Italy
[3]Politecnico di Torino, Mechanical and Aerospace Engineering Dep., Torino, Italy
*f.degregorio@cira.it

Abstract. The aim of the article is to propose a robust and reliable engineering method for identifying and characterizing vortical structures within a flow field measured with a classic two-component PIV measurement system. Some of the most popular vortex-detection criteria are briefly presented for comparison purposes. Many of these fail if spurious vectors are present within the flow field due to poor PIV image quality. The proposed method was tested both on synthetic images of ideal vortices, having different spatial resolutions and different noise levels in order to perform a parametric assessment, and on real PIV images of a four-bladed rotor wake.

1 Introduction

Many engineering applications deal with flows characterized by vortices. In particular, in the aeronautical field the study of the aerodynamic characteristics of new fixed wing or rotary wing vehicles requires the identification and characterization of such structures. In the recent years, PIV became the state of art technique for the velocity field measurement in the rotorcraft field [1],[2].

Despite the concept of vortex is a well-known and intuitive flow phenomenon, present in many natural events and well investigated in fluid mechanics, a universally accepted definition is still missing. A first possible definition of vortex was given by Lugt [3]: "a vortex is the rotating motion of a multitude of material particles around a common centre''. About ten years later, Robinson [4] stated that "a vortex exists when the instantaneous flow lines in the normal plane to the nucleus of the vortex, placed a moving observer together with the centre of the nucleus itself, exhibit a roughly circular or spiral movement". Although the definition of vortex is very ambiguous, several criteria have been developed for the identification of vortices over the years as discussed by Chakraborty et al [5], Kolar [6] and lately by Epps [7]. In the classical theory of fluid mechanics, vortices are often thought of as regions of high vorticity, and for this reason several researchers have long applied a vorticity threshold criterion to identify the vortices where the connected region has vorticity over a given threshold [7]. Similarly, being the circulation linked to vorticity through the Stokes theorem, also the circulation was widely used as a criterion for vortex detection. In our days, the most used local methods for vortex identification are based on the analysis of the velocity-gradient tensor $\nabla \boldsymbol{v}$, its symmetric and antisymmetric parts, strain rate tensor $\mathbf{S}$ and vorticity tensor $\boldsymbol{\Omega}$, respectively, and the three invariants of $\nabla \boldsymbol{v}$. The paper presents the main vortex identification methods based on the velocity gradient tensor as: the Q criterion proposed by Hunt et al [8]; the Δ criterion introduced by Dallmann [9], Vollmers et al. [10], and Chong et al. [11]; the maximum of the vorticity and the maximum of the circulation [12]. These local vortex detection criteria are not always suitable for PIV data, affected by noise and spurious vector resulting in high velocity gradients. A possible solution was offered by the Γ_2-criterion proposed by Graftieaux et al. [13] and successfully applied to complex dynamic stall measurements on highly separated flow by Mulleners and Raffel [14]. The paper briefly illustrates in Section 2 some of the most popular vortex detection

criteria together with the most promising Γ_2 method. Some synthetic images of theoretical vortices and some real PIV images of experimental test campaign have been used as test cases. The synthetic images were generated with different spatial resolutions, sizes, and noise levels in order to perform a parametric and comparative study. These results are described in Section 3.

The real images include two characteristic cases: the presence of a body within the measurement field of view and a highly turbulent flow considered as a sort of noise for the identification process. The obtained results are fully discussed in Section 4 and the main conclusions are drawn and illustrated in Section 5.

2 Vortex-identification schemes

In the following some selected techniques widely used in literature are briefly presented in their essential characteristics with particular attention to the Γ_2 method.

2.1 Maximum Vorticity Criterion

The vorticity $\vec{\omega} = \nabla \times \vec{v}$ reaches a local maximum in the centre of the vortex, so this feature can be exploited to identify the centre of the vortex. In 1991, Robinson [4] pointed out that the vorticity is unable to distinguish between a real rotation region and a shear layer region, and that the maximum magnitude of the vorticity does not necessarily occur in the central region of vortex structures. Although this criterion can be very misleading, the vorticity is often used as a first approximation to detect and evaluate the intensity of a vortex.

2.2 Maximum of circulation criterion

The circulation γ reaches a local maximum in the centre of the vortex, so this feature can be exploited to identify the centre of the vortex. The circulation has been calculated following the method suggested by Vollmers [12].

2.3 Q-criterion

Hunt et al. [8] identify vortices of an incompressible flow as connected fluid regions with a positive second invariant of ∇u

$$Q = -\frac{1}{2}\left(u_x^2 + v_y^2 + w_z^2 + 2\,u_y v_x + 2\,u_z w_x + 2\,v_z w_y\right) = \frac{1}{2}\left(\left\|\bar{\bar{\Omega}}\right\|^2 - \left\|\bar{\bar{S}}\right\|^2\right) > 0 \qquad (1)$$

that is, as the regions where the vorticity magnitude prevails over the strain-rate magnitude. In addition, the pressure in the vortex region is required to be lower than the ambient pressure.

2.4 Δ-criterion

Dallmann [9], Vollmers et al. [10] and Chong et al. [11] define vortices as the regions in which the eigenvalues of ∇u are complex (a pair of complex-conjugate eigenvalues occurs) and the streamline pattern is spiralling or closed in a local reference frame moving with the point. Such points can be viewed within the critical-point theory – on a plane spanned by the complex eigenvectors – as elliptic ones (focus or centre). For incompressible flows, this requirement reads:

$$\Delta = \left(\frac{1}{2}\,R\right)^2 + \left(\frac{1}{3}\,Q\right)^3 > 0 \qquad (2)$$

where Q and R are the invariants of ∇u, Q is given by eq. (1), $R = \det(\nabla\vec{v})$. Q and R play a key role in the reduced (due to incompressibility) characteristic equation for the eigenvalues λ of ∇u:

$$\lambda^3 + Q\lambda - R = 0 \qquad (3)$$

2.5 Γ_2-criterion

The most widely used local methods for vortex identification are based on the analysis of the velocity-gradient tensor and its three invariants. In some cases, these local vortex-detection criteria are not suitable for PIV data, as for example in the regions affected by blade passages or the lower part of the rotor downwash where the tip vortex spirals are concentrated and the flow is highly turbulent. The

possible solution is offered by the Γ_2 criterion proposed by Michard and Favelier [15]. The function Γ_2 is defined in discrete form as:

$$\Gamma_2(\vec{x_i}) = \frac{1}{M}\sum_{x_j \in S_i} \frac{\{(\vec{x_j}-\vec{x_i})\times(\vec{u}_j-\vec{u}_{mean})\}\cdot\vec{n}}{|\vec{x_j}-\vec{x_i}||(\vec{u}_j-\vec{u}_{mean})|} \quad (4)$$

with S_i a two-dimensional circle around x_i with radius D, M the number of grid points x_j inside S_i with $j \neq i$, $\vec{n}$ the unit normal vector and u_j the velocity at x_j. According to its definition, Γ_2 is a 3D dimensionless scalar function, with $-1 \leq \Gamma_2 \leq 1$. The zones delimited by $|\Gamma_2| > \frac{2}{\pi}$ identify the vortices depicted by the measurement region. The vortex centre is identified as the maximum of the absolute value of Γ_2 in the delimited zone. For each identified vortex, the centre position is measured and the main characteristics, in terms of swirl velocity, vorticity and circulation are calculated along the vortex radius. The choice of the domain radius D have an influence on the dimension of the identified vortices and on the accuracy of the centre detection. In order to assess the reliability of the criteria a parametric investigation is performed using a single or a pair of vortices.

3 Test Cases

3.1 Synthetic Vortex

In order to assess the reliability of the Γ_2 criterion, a parametric investigation was carried out by using numerically-generated velocity fields containing a single (main, indicated by V_1) or a couple (main plus secondary, named V_2) of theoretical vortices, co-rotating or counter rotating. In particular, the Vatistas [16] vortex core model was used for the purpose, according to which the swirl velocity is expressed as:

$$V_\theta = \frac{\Gamma}{2\pi}\left[\frac{r}{(r^{2n}+{r_c}^{2n})^{\frac{1}{n}}}\right] \quad (5)$$

This model was normalized with respect to $\frac{|\Gamma_1|}{2\pi}$, being $|\Gamma_1|$ the module of the circulation of the main vortex, and its core radius r_{c1}, thus yielding the expression:

$$\bar{V}_\theta = \frac{\Gamma}{|\Gamma_1|\, r_{c1}}\left[\frac{\bar{r}}{(\bar{r}^{2n}+\rho^{2n})^{\frac{1}{n}}}\right] \quad (6)$$

where $\bar{r} = r/r_{c1}$, $\rho = r_c/r_{c1}$ and the coefficient n was set equal to "1.06" as suggested by Scully [17].

The capability of the criteria to detect vortices, even in the presence of white noise backgrounds, and to take into account the influence of a secondary vortex in the flow field, was tested by generating several velocity fields on a squared XY Cartesian grid. The computations were performed by varying: the spatial resolution of the grid ($\Delta L/r_c$=0.5, 0.2, 0.1 and 0.05); the strength of the secondary vortex $\frac{\Gamma_2}{|\Gamma_1|} = [\mp 0.5;\ \mp 1;\ \mp 2]$; the distance of the secondary vortex with respect to the main one; the amplitude of the white noise background, expressed as a percentage of the maximum value of the swirl velocity of an isolated vortex of unit strength ($V_{\theta,max} \sim 0.52$). At the same time, the local vortex-identification criteria based on the velocity gradient were applied for comparison.

3.2 Four-bladed rotor set-up

A dedicated rotor test rig was developed in the framework of the GARTEUR AG22 activities [18] (Visingardi et al 2017) based on an existing commercial radio-controlled helicopter model (Blade 450 3D RTF), but largely customized and modified for the scope of the experiment, Figure 1. A four-bladed rotor with collective and cyclic control replaced the original two-bladed rotor hub. The rotor presented four untwisted, rectangular blades with radius of R=0.36 m, root cut-out at 16% of the radius, chord length of c=0.0327m and a NACA0013 airfoil throughout the blade span [19]. The resulting rotor solidity value was equal to σ=0.116. The clockwise rotor maximum speed was Ω=1780 rpm, and the collective pitch angle θ_0 varied from 1 to 11.3 degree.

The rotor downwash characteristics were measured by a standard two components measurement system composed by a double head Nd-Yag laser with a maximum energy of 320 mJ per pulse at 532 nm and a single double frame CCD camera (2048 by 2048 px). In order to track the blade tip vortices in the proximity to the rotor disk, measurement were performed using a 200 mm focal length obtaining a field of view of about 120 x 120 mm^2 and an optical resolution was about 17 px/mm. The time delay between the laser double–pulses was 25 μs. The results presented a velocity spatial resolution of Δx=0.93 mm. The random noise of the PIV cross–correlation procedure can be estimated as 0.1 px as a rule–of–thumb. Using the current values for the optical resolution (17 px/mm) and the laser double–pulse delay (25 μs), this related to a velocity error of ΔV of ~ 0.23 m/s for the tip vortex measurements.

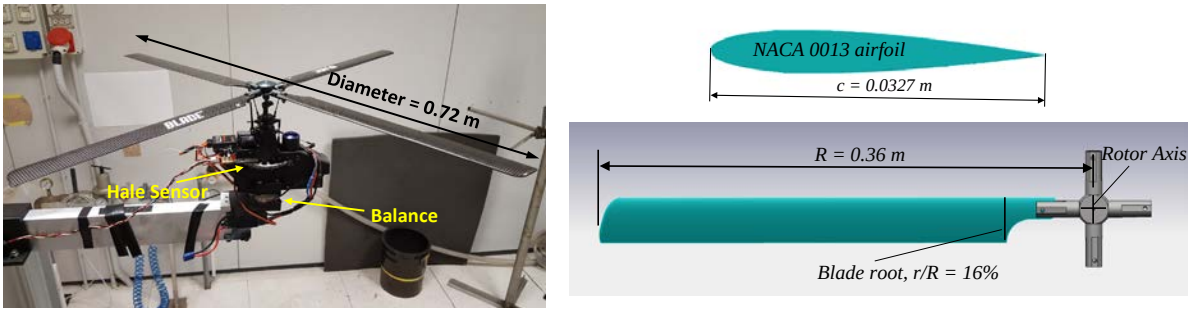

Figure 1. Rotor test rig (left image) and airfoil and planform blade drawings (right image).

The measured blade tip vortex core radius (defined as the distance from the vortex centre to the radial position where the maximum tangential velocity is reached) was between 3mm to 3.3mm so that the ratio $\Delta x / r_c$ was of about 0.31-0.28 and comparable with the limit value of $\Delta x/r_c \leq 0.2$ indicated by Martin et al. [20] in order to assure a correct vortex characterization. In particular, the vortex identification criteria are tested in proximity of the rotor blade where the tip vortex are well defined but the blade can lay in the field of view inducing strong reflection (Figure 2-b) and at about one radius downstream the rotor disk where strong instability is present and the velocity fluctuation increases (Figure 2-c)

.

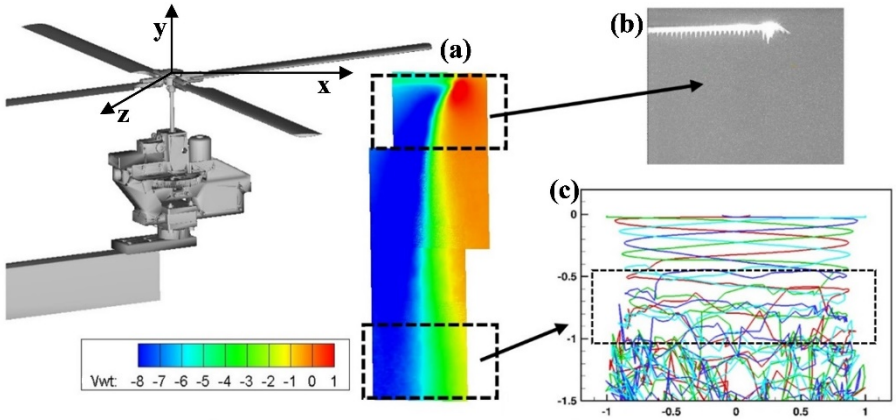

Figure 2. Rotor rig: a) downwash; b) PIV image with blade laser reflection; c) blade tip vortices path.

4 Results

4.1 Single synthetic vortex

The single normalized Vatistas vortex is centred in the origin of the Cartesian axis, has core radius equal to r_c=1, circulation $\gamma=2\pi$, maximum swirl velocity V_θ=0.52 and the velocity field size is 20 by 20 times the core radius. The parametric study foresaw the investigation of the single vortex for different spatial resolutions ($\Delta L/r_c$ = 0.5, 0.2, 0.1, 0.05) and with different white noise levels (0%, 20%, 50%, 70%, 90%). The Γ_2 criterion is applied varying the domain radius D in the range from 2 to 20 in order to find

a relationship between the domain radius and the image spatial resolution. The main characteristics of the synthetic single vortex are summarised in Table 1 for different spatial resolutions.

Table 1. Main characteristics of a single synthetic vortex.

$\Delta L/r_c$	0.5	0.2	0.1	0.05
r_c	1	1	1	1
Γ	2π	2π	2π	2π
Velocity field size	40x40	100x100	200x200	400x400
N. of samples in r_c	2	5	10	20

The Γ_2 criterion accurately detects the correct centre of the synthetic single vortex without noise for any spatial resolution and any selected domain radius D. It is worth noting that the smallest domain radius (D=2) provides the most accurate results and increasing the domain radius the Γ_2 peak value increases together with the domain radius D approaching the unit value (Table 2). Unlike what stated by Graftieaux et al. [13], it is shown that Γ_2 function is influenced by the choice of the domain radius (Figure 3) and therefore cannot be used to delimit the vortex core radius. For this reason, in the present study, once the centre has been identified, the tangential velocity is calculated on concentric centres increasing the radial distance from the centre: the core radius r_c is identified as the point with the maximum swirl speed and not as the radius of the circular region corresponding to $\Gamma_2 = 2/\pi$.

Table 2. Vortex centre detection. Maximum of Γ_2 and V_θ, and radius core variation with the domain radius D.

D	x	y	Γ_2 max	r_c	V_θ max
2	0.00	-3.80E-18	-0.913	1.005	0.519
5	0.00	6.45E-18	-0.978	1.005	0.519
10	0.00	2.30E-17	-0.993	1.005	0.519
20	0.00	4.47E-17	-0.998	1.005	0.519

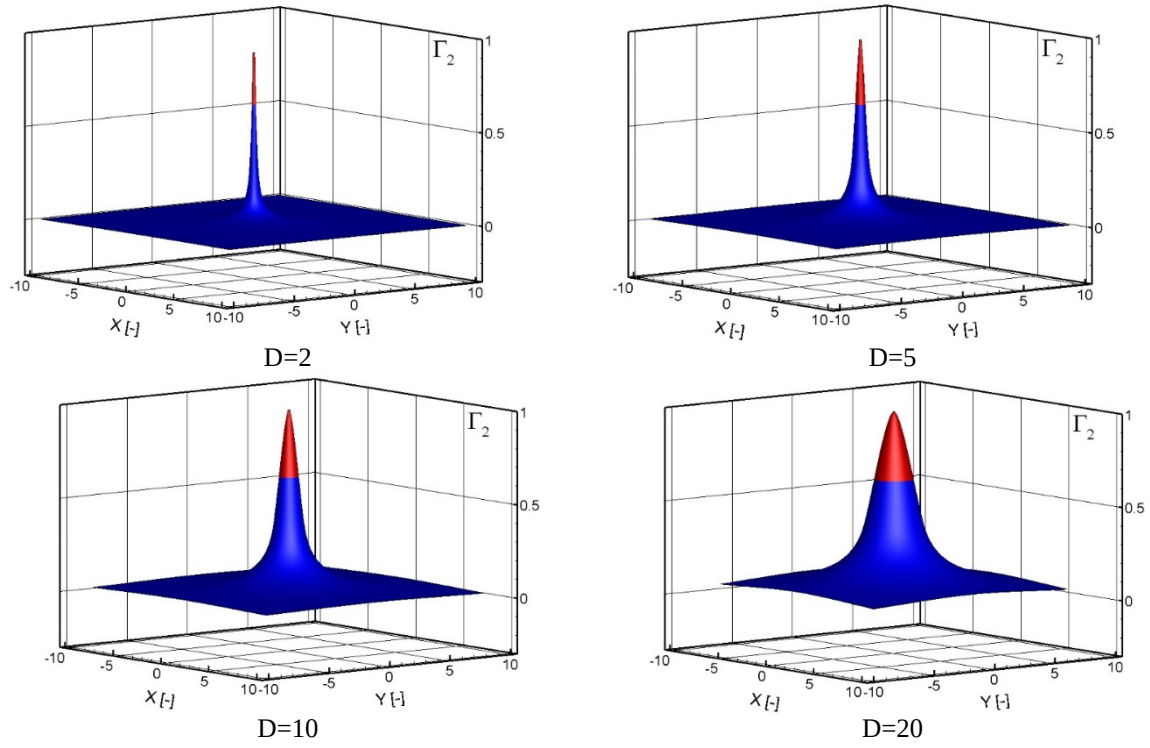

D=2 D=5

D=10 D=20

Figure 3. Γ_2 functions of a single vortex with spatial resolution $\Delta L/r_c$=0.1 for different domain radii.

The swirl velocity trend is plotted as the spatial resolution varies together with the theoretical Vatistas curve (Figure 4). The obtained maximum swirl velocity data indicate a negligible error with respect to the theoretical curve except for the case with spatial resolution $\Delta L/r_c$=0.5, where the error is about the 4% of the maximum speed being the spatial resolution larger than the limit of $\Delta L/r_c$=0.2 indicated by Martin [20]. Similarly, the other vortex-detection criteria also correctly identify the centre of the vortices and the characteristics.

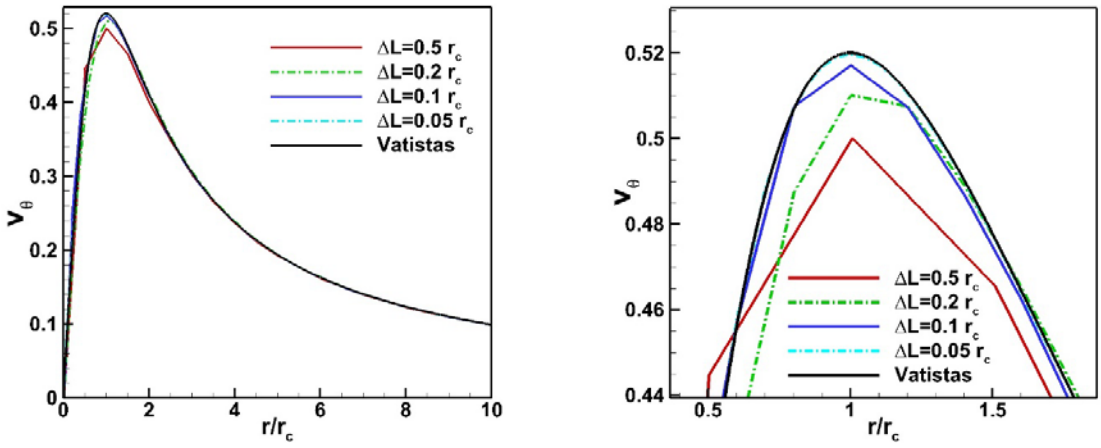

Figure 4. V_θ vs normalized radius for different spatial resolutions and zoom of peak region.

The analysis of the synthetic images with different levels of noise provides information on the relationship between the vortex core spatial resolution and the correct value of the Γ_2 radius to be set. The measurement percentage error $\varepsilon(d_c)$ of the vortex centre is defined as $\varepsilon(d_c)\% = \frac{\sqrt{\Delta x_c^2+\Delta y_c^2}}{\sqrt{\Delta x^2+\Delta y^2}}\%$ where Δx_c and Δy_c are the axial components of the detected centre distance to the theoretical centre and Δx and Δy are the components of the spatial resolution. In the current case, being the velocity matrix equally-spaced, the formula becomes $\varepsilon(d_c) = \frac{\sqrt{\Delta x_c^2+\Delta y_c^2}}{\Delta L\sqrt{2}}\%$. An error smaller than the 70% indicates that the detected centre falls inside the same cell grid of the theoretical vortex. A value equal or larger than 100% indicates that the distance from the theoretical vortex is larger than the diagonal of the velocity grid.

The Γ_2-criterion results indicate that increasing the noise level of the synthetic images, the smaller value of the radius fails in detecting the vortex centre.

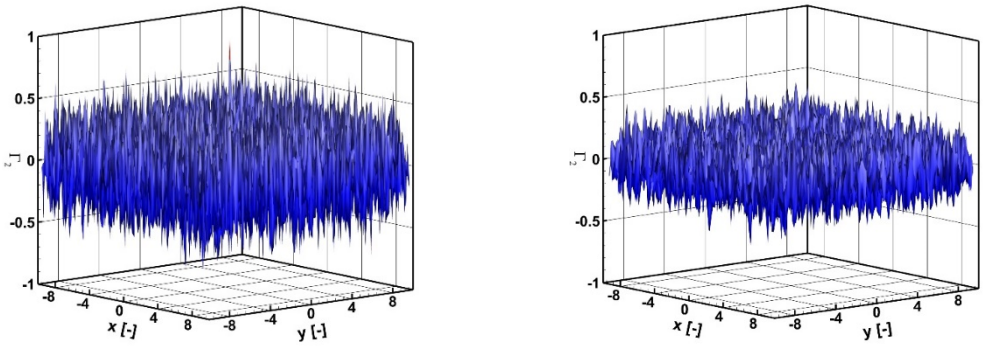

D=2 D=3

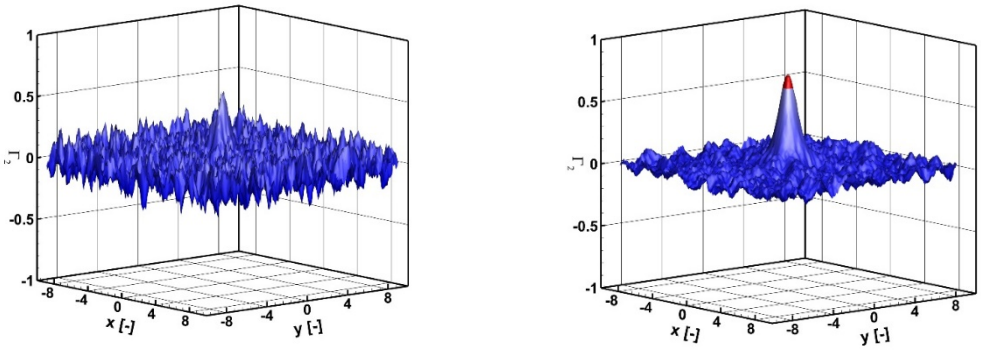

Figure 5. Γ_2 functions for different radii of a synthetic vortex with $\Delta L/r_c$=0.1 and 90% noise.

The Γ_2 function becomes too sensitive to the noise for small radius values at which presents several erroneous peaks or does not reach the threshold value (Figure 5). The best result is obtained setting the domain radius equal to the number of sample points present along the core radius. Table 3 summarises the detection centre error values of the Γ_2 criterion for a fixed spatial resolution of $\Delta L/r_c$=0.1 and varying the domain radii and the noise levels. For each noise level, the minimum error is obtained for D=10, while further increasing the domain radius, the error slightly increases.

Table 3. Vortex centre detection error $\varepsilon(d_c)$% for spatial resolution of $\Delta L/r_c$ =0.1 for different noise levels.

D	2	3	5	10	15	25
Noise: 0%	0.1%	0.1%	0.1%	0.1%	0.1%	0.2%
Noise: 20%	34.9%	2.9%	0.8%	0.5%	0.5%	11.1%
Noise: 70%	\	\	36.1%	1.5%	2.4%	8.7%
Noise: 90%	\	\	\	35.1%	46.9%	36.6%

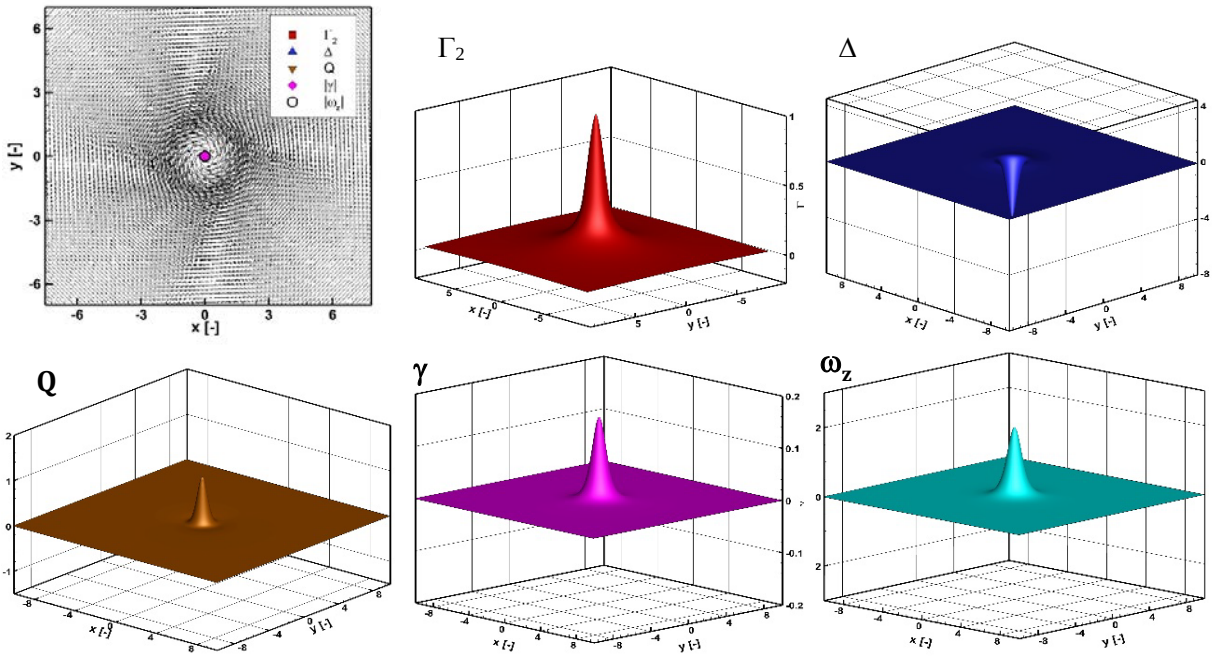

Figure 6. Vatistas Vortex - Velocity field and detected centres with different criteria: Noise 0%.

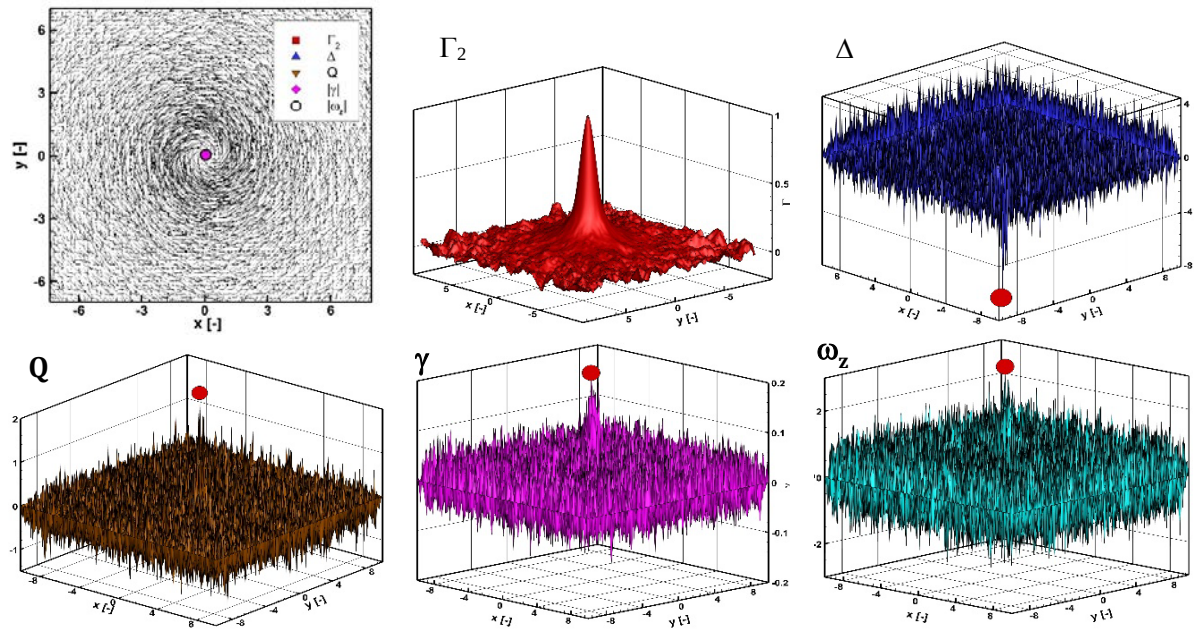

Figure 7. Vatistas Vortex - Velocity field and detected centres with different criteria: Noise 20%.

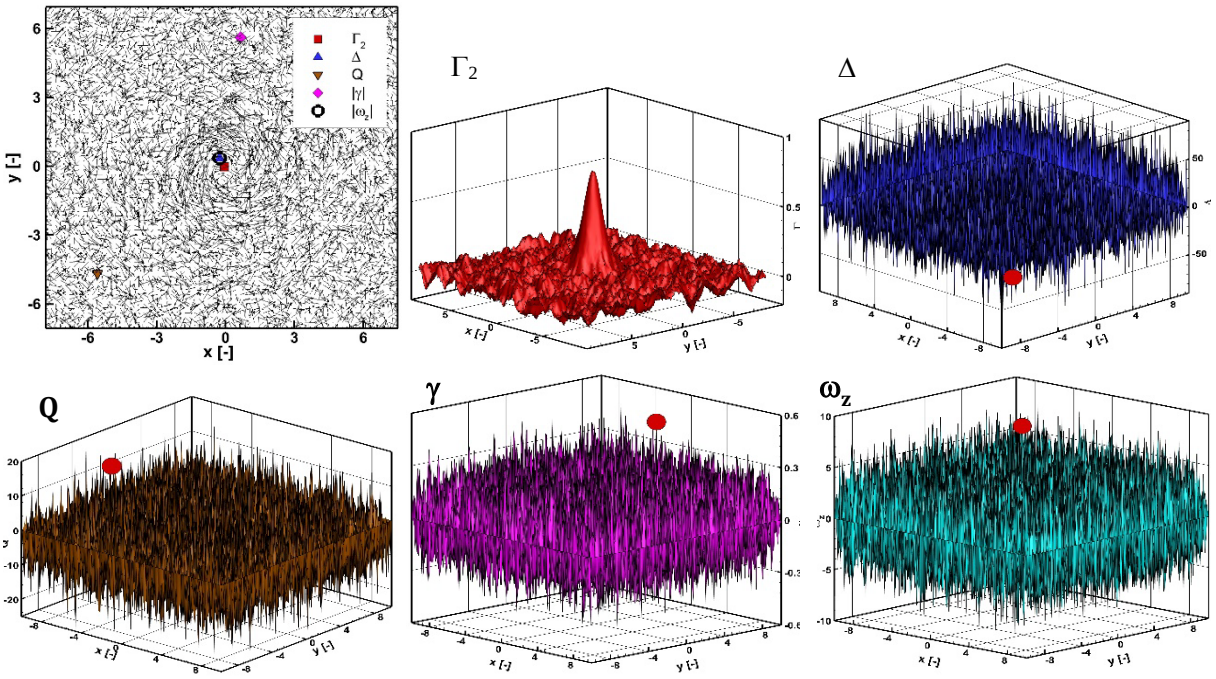

Figure 8. Vatistas Vortex: Velocity field and detected centres with different criteria. Noise 70 or 90%.

In comparison with the other selected methods, the Γ_2 criterion provides the best results in identifying the centre of the vortex as the noise level increases. Without noise or for a 20% of noise all criteria correctly identify the centre (Figure 6 and Figure 7). For noise of 70%, the Δ and Q criteria detect the centre three mesh cells far from the correct position whereas the circulation γ-criterion is completely mistaken. For the case with noise of 90%, the Δ and ω_z criteria miss the identification of the vortex of about four mesh cells whereas the Q and γ criteria completely fail to detect the correct centre, as shown in Figure 8. Table 4 summaries the centre location error for the different criteria and noise levels.

Table 4. Vortex centre detection error $\varepsilon(d_c)$ of the different criteria by varying the noise level.

Criterion	Γ_2	Δ	Q	ω_z	γ
Noise: 20%	0.5%	43.8%	17.9	51.7%	10.6%
Noise: 70%	1.5%	181.2%	181.2%	49.0%	7385.0%
Noise: 90%	35.1%	305.7%	5145.5%	305.7%	4003.3%

For the sake of completeness, the above mentioned figures shows the functions obtained by the different vortex identification criteria for different noise levels in order to give a clear picture of the criteria sensitivity to the noise. Once that the centre is located (red circle), the main vortex characteristics are calculated by the velocity matrix.

In particular, Figure 9 shows the swirl velocity calculated by all the criteria for noise of 0%, 20% and 90%, respectively. Figure 9-c presents the effect of the wrong centre location. The swirl velocity calculated starting from the wrong centre positions provided by Q and γ criteria display an incorrect behaviour.

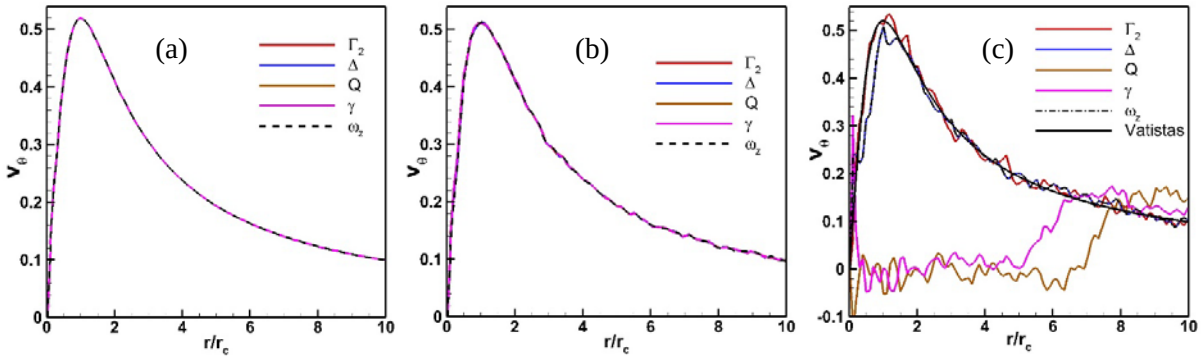

Figure 9. Vatistas Vortex. Swirl velocity vs radial distance with different criteria. Noise 0% (a), noise 20% (b) and noise 90% (c).

4.2 Multiple Synthetic Vortex

The reliability of the vortex detection criteria was investigated on multiple vortices or on a single elliptical vortex obtained by merging two circular vortices. The test cases were set up by coupling two single vortices. The main vortex V_1 was maintained constant, with centre located in x_1=-3 and y_1=0, core radius r_c=1, circulation $\gamma_1=2\pi$, swirl velocity of V_θ=0.52 and spatial resolution of $\Delta L/r_c$=0.2. The secondary vortex was varied in terms of circulation intensity γ_2, dimension r_{c2} and position (x_2, y_2=0).

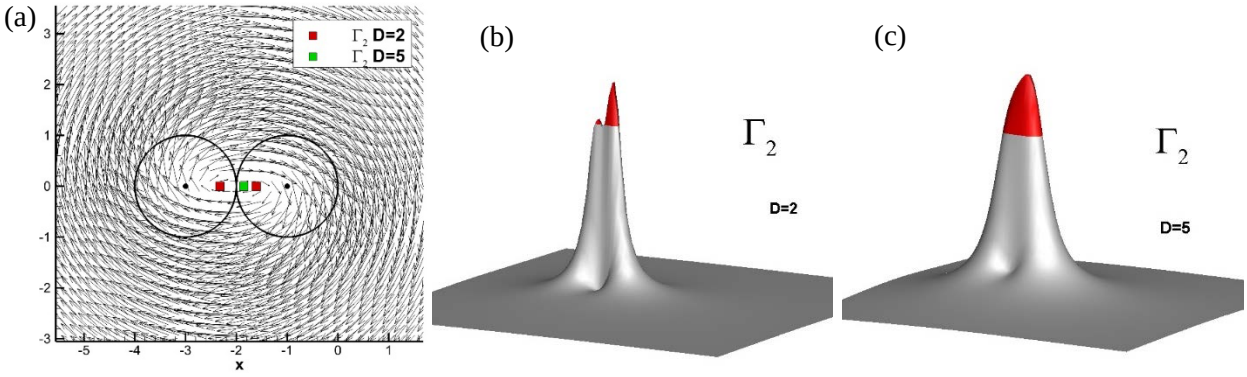

$r_2=r_1$, $\gamma_2=\gamma_1$ and $d=r_1+r_2$ Γ_2 -criterion $D=2$ Γ_2 -criterion $D=5$

Figure 10. Case 1: Merging elliptical vortex, domain radius effect.

A number of 54 test cases was generated of which 31 cases merged in a single vortex and the remaining showed a couple of vortices. Case 1 was obtained selecting the secondary vortex to be tangent to the main one, having same circulation and core radius. The resulting velocity fields presented a single elliptical vortex (Figure 10-a). The Γ_2-criterion calculated with the domain radius D=2 showed a double peak function detecting two vortex centres (Figure 10-b) whereas increasing the radius value to D=5 a single vortex was depicted (Figure 10-c). The results suggest the use of a value of the domain radius of the same order as the core radius in order to correctly detect the centre of the vortex. Smaller values provide two separated vortices.

Case 2 presents a pair of contra-rotating vortices obtained by setting the secondary vortex tangent to the main one, with same radius and circulation but opposite sense of rotation. The opposite senses of rotation prevent the merging of the two vortices by keeping them apart and distinct (Figure 11). In this case, both values of the Γ_2 domain correctly detect the vortex centres and similarly to the single clean vortex, the smaller domain radius provides the best result.

Case 3 shows two vortices of different intensity obtained by coupling with the main vortex a secondary vortex located in x_2=+3 and y_2=0 characterised by larger radius $r_{c2}=3r_{c1}$, stronger circulation and opposite direction $\gamma_2=-4\pi$. The resulting velocity field presents two distinct vortices of different intensity. The Γ_2-criterion correctly detects the vortex centres for both domain values (Figure 12).

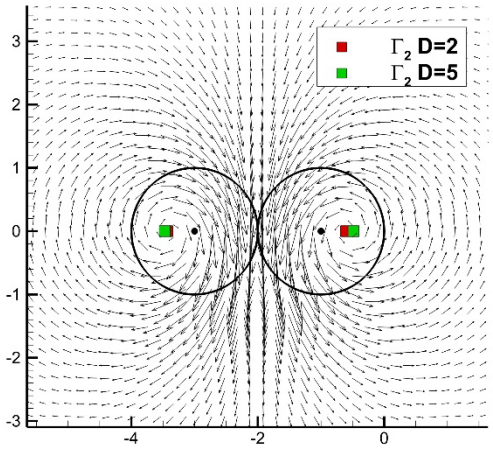

$r_2=r_1$, $\gamma_2=-\gamma_1$ and $d=r_1+r_2$

Figure 11. Case 2: Tangent contra-rotating vortex pair with Γ_2 detected vortices for different domain radii.

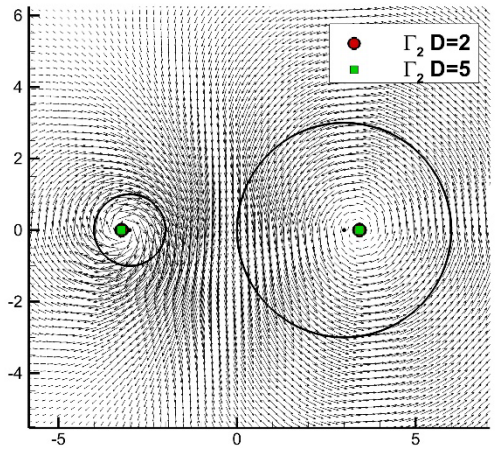

$r_2=3r_1$, $\gamma_2=-2\gamma_1$ and $d>r_1+r_2$

Figure 12. Case 3: Distant contra-rotating vortex pair with Γ_2 detected vortices for different domain radii.

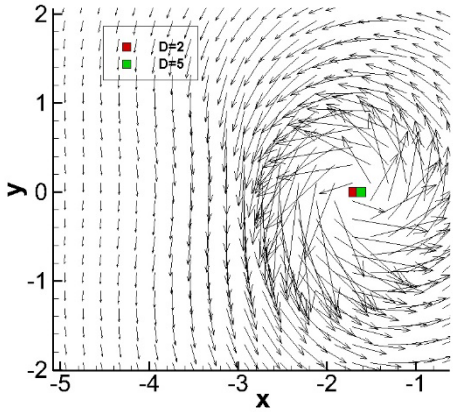

Figure 13. Case 4: $r_2=0.5r_1$, $\gamma_2=-2\gamma_1$, $x_2=-1.75$ and $d<r_1+r_2$.

Case 4 couples two contra-rotating vortices with the secondary one located close to the main vortex at x_2=-1.75 and characterised by stronger intensity γ_2=-2γ_1 and smaller radius r_2=0.5r_1. The secondary vortex annihilates the main one. The Γ_2–criterion detects a single vortex in the resulting velocity field (Figure 13) and both domain radii provide the correct centre position.

The other criteria were applied for comparison only for the cases 2 and 4. For the case 2, characterised by equal contra-rotating vortex pairs, happens that all the other criteria detect the centre position in the proximity to the source vortex position instead locating the centre in the new position coming from the mutual vortex interaction (Figure 14). For the case 4, Δ, Q, ω_z and γ criteria correctly detect the position of the secondary vortex but indicate the erroneous presence of another vortex in the proximity to the main vortex at about x=-3.2 and x=-3.4 (Figure 15).

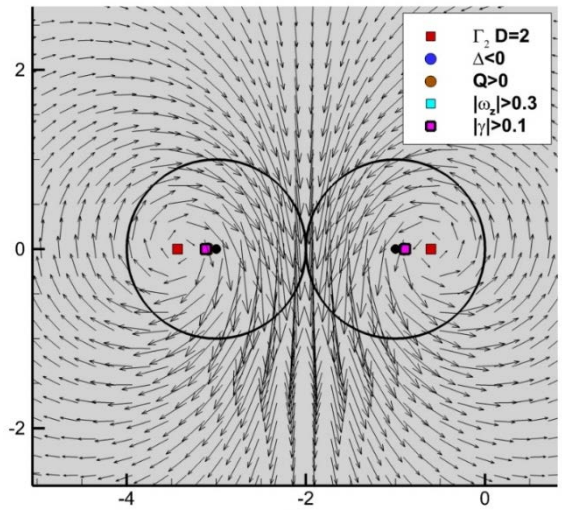

r_2=r_1, γ_2=-γ_1 and d=r_1+r_2

Figure 14. Case 2: Different criteria comparison.

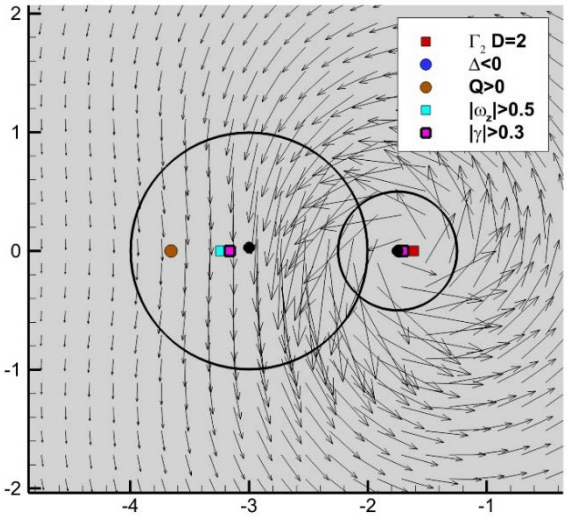

r_2=0.5r_1, γ_2=-2γ_1, x_2=-1.75 and d<r_1+r_2

Figure 15. Case 4: Different criteria comparison.

The reliability of the Γ_2-criterion in detecting the vortex centres was tested on a velocity field containing two vortices with great difference of intensity. The case 5 was obtained by coupling to the main vortex a second counter-rotating vortex located at x_2=0.5, having radius equal to r_{c2}=3r_{c1} and larger circulation γ_2=-2γ_1. The resulting velocity field shows a more intense vortex at about x_1=-3.43 and a weaker vortex at about x_2=1.41.

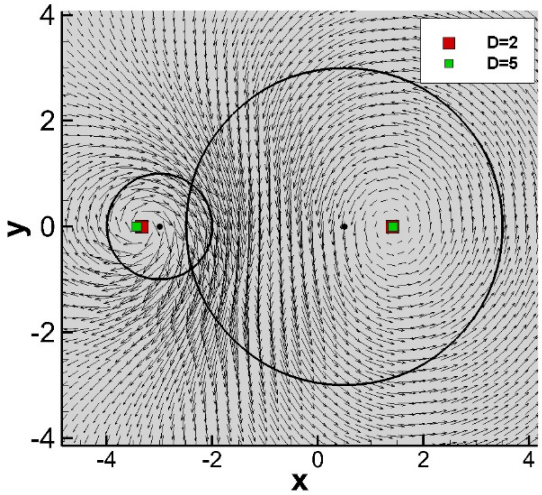

Figure 16. Case 5: $r_{c2} = 3r_{c1}$, $\gamma_2 = -2\gamma_1$, d < $r_1 + r_2$.

The main vortex is better described by the smaller domain radius D=2 whereas the larger one is correctly detected by both. The Γ_2 detection criterion was also investigated adding white noise level of 50 and 90% to the case 5. Different domain radii, from D=2 to D=15, were applied. For a white noise value of 50%, the first vortex is always detected and the smallest detection error of $\varepsilon(d_c)$=5% is obtained for D=12 (Table 5). Figure 17 a and b depicts the Γ_2 behaviour with 50% of noise for D=5 and D=15, respectively. The smaller domain is able to detect the first vortex but the second is shaded by the noise. Increasing the domain to D=15, the two peaks are visible and the threshold value is reached (blue coloured in Figure 17-b). Further increasing the noise up to 90%, the first vortex is detected for domain values up to D=7 whereas the second vortex never reaches the threshold value $\Gamma_2=2/\pi$ (Table 5). The two peaks are clearly detectable in Figure 17-d but the threshold value is not reached.

Table 5. Vortex centre detection error for different domain radius and white noise for case 5.

Noise	*D=2*	*D=3*	*D=5*	*D=7*	*D=12*	*D=15*
20% (x_1, y_1)	19%	26%	31%	39%	103%	116%
20% (x_2, y_2)	\	81%	72%	30%	52%	83%
50% (x_1, y_1)	64%	46%	22%	8%	5%	28%
50% (x_2, y_2)	\	\	\	\	45%	5%
90% (x_1, y_1)	82%	82%	65%	69%	\	\
90% (x_2, y_2)	\	\	\	\	\	\

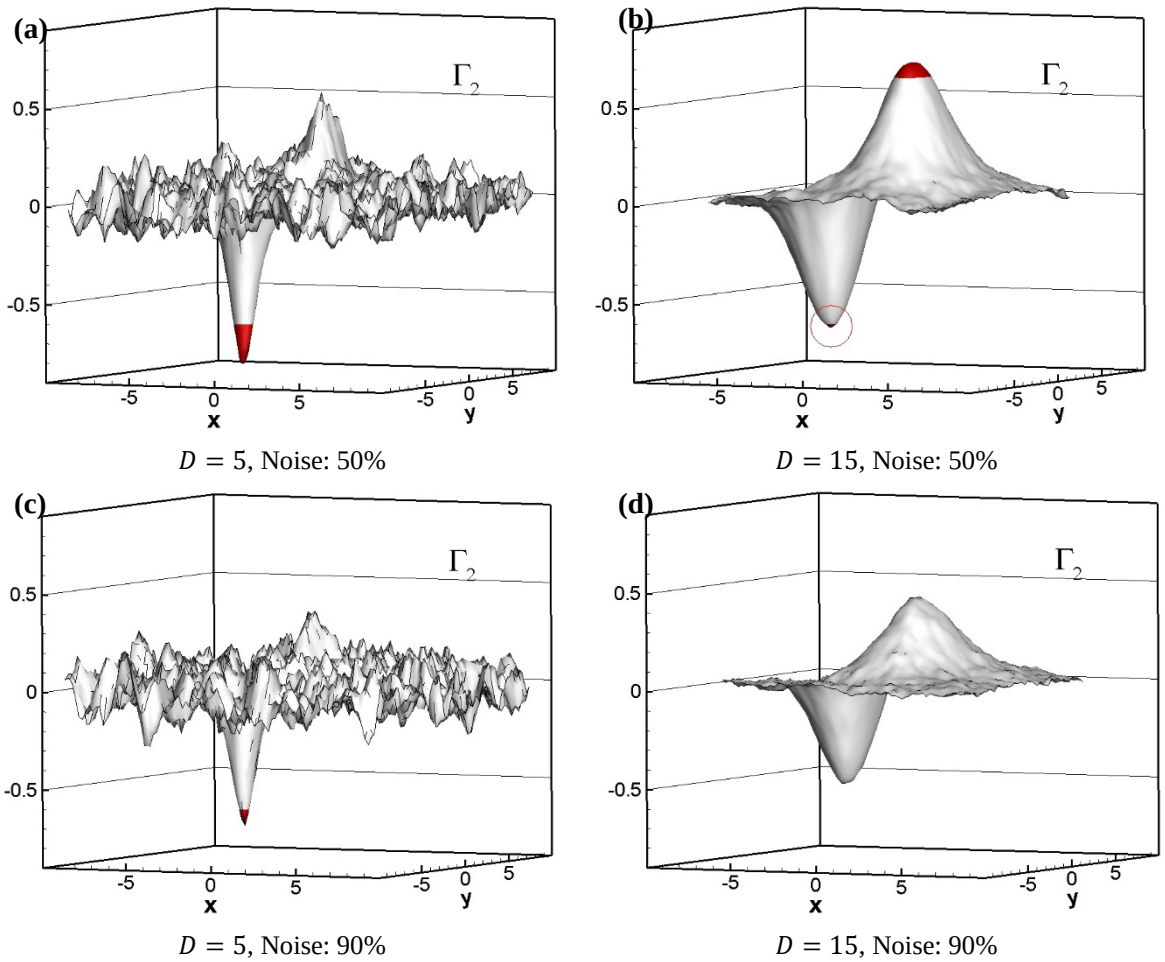

$D = 5$, Noise: 50% $D = 15$, Noise: 50%

$D = 5$, Noise: 90% $D = 15$, Noise: 90%

Figure 17. Γ_2 –criteria for case 5 varying noise and domain radius

Case 5 investigates the behaviour of the other vortex detection criteria in case of spurious vectors. Table 6 summarises the vortex detection centre error for all the investigated criteria. The Γ_2-criterion provides the best results in terms of accuracy in detecting the vortex centre and it is the most robust to the spurious vectors. For Γ_2, the detection centre error remains confined in a cell grid on both vortices except for the case with 90% of noise where the vortex centre is not validated on the secondary vortex. For noise of 20% and the first vortex, the Δ, Q and γ criteria locate the centre at one diagonal distance from the correct value whereas the vorticity ω_z identifies the centre in the same cell grid. For the weaker vortex, the other criteria fails in detecting the centre, best results are provided by the circulation criterion that presents an error of $\varepsilon(d_c)$=195%.

For the noise level of 50%, the first vortex detection error is confined inside a grid cell for Δ, Q and ω_z. The circulation locates the centre at a diagonal cell distance. All the criteria fail to identify the centre.

For the noise level of 90% only the circulation criterion is able to detect the first vortex with a limited error of $\varepsilon(d_c)$=67%. The other criteria miss the centre detection for both vortices. The velocity fields with and without white noise are reported in Figure 18 together with the location of the centres calculated by all the investigated criteria.

Table 6. Vortex detection centre error for case 5: $r_2=3r_1$, $\gamma_2=-2\gamma_1$ and $d<r_1+r_2$.

Noise		Γ_2	$\Delta < 0$	$Q > 0$	$\lvert\omega_z\rvert$>0.15	$\lvert\gamma\rvert$ >0.1
20%	(x_1, y_1)	19%	116%	116%	45%	102%
	(x_2, y_2)	30%	703%	703%	243%	195%
50%	(x_1, y_1)	5%	79%	79%	78%	123%
	(x_2, y_2)	5%	271%	4092%	751%	3436%
90%	(x_1, y_1)	65%	2443%	3305%	149%	67%
	(x_2, y_2)	\	444%	440%	431%	2833%

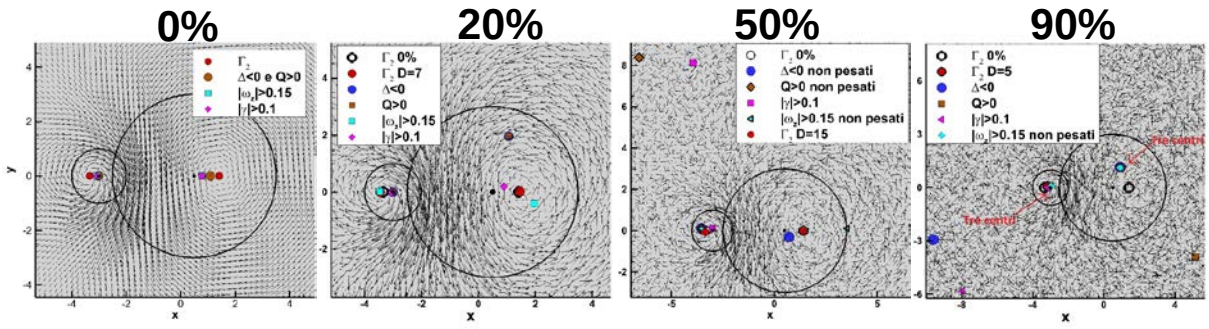

Figure 18. Case 5 velocity fields with different noise levels.

4.3 Rotor Blade Tip Vortices

A typical event that is faced in the case of measurements on rotors, propellers or windmills, is the blade passage in the measurement area (Figure 19-a). This involves the presence of strong laser reflections, which reduce the quality of the measurements and generate a large number of spurious vectors (Figure 19-b) thus invalidating the application of the vortex identification methods based on the velocity gradient. The Q-criterion shows a large number of strong peaks distributed along the path of the rotor blade whereas the tip vortices are depicted by weaker peaks and consequently not validated as shown in Figure 20-a. Analogous behaviour is obtained by Δ, ω_z and γ criteria, positioning all the centres on the blade trajectory.

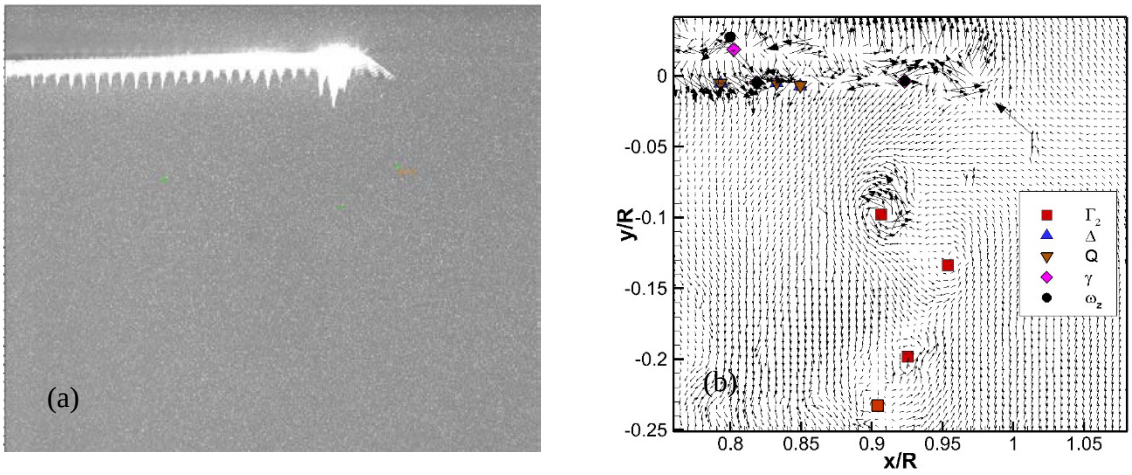

Figure 19. PIV image characterized by rotor blade passage (a) and related velocity field (b).

The Γ_2-criterion also perceives the presence of the blade showing a series of peaks that however not reach the threshold value $\left(\Gamma_2 < \frac{2}{\pi}\right)$. On the contrary, the tip vortices are detected and validated by intense peaks that exceed the threshold value $\left(\Gamma_2 > \frac{2}{\pi}\right)$ and red coloured in Figure 20-b. This characteristic allows to investigate the rotor wake behaviour without applying time consuming image masking procedures or expensive in terms of calculations as the POD-based background removal techniques [21].

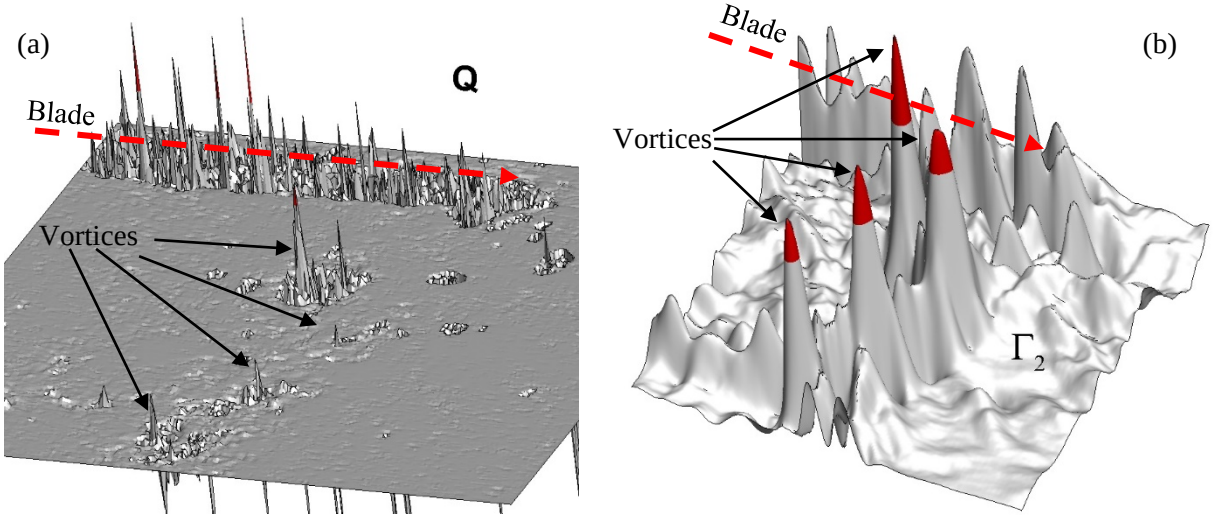

Figure 20. Blade passage: a) Q-criterion; b) Γ_2-criterion.

The second test case is selected at a distance of about one radius downstream the rotor disc, a region characterized by high turbulent flow due to the interaction of the blade tip vortices. The Q-criterion identifies correctly the vortical structures in the velocity fields as shown in Figure 21-a, but the peaks of the vortex are exceeded in intensity by spurious peaks that do not allow their identification. The majority of the peaks are located on the lower left side of the flow velocity and marked by red circular markers. The Γ_2-criterion validates three main peaks exceeding the threshold value of $2 / \pi$ and red coloured in the Figure 21-b. The Γ_2 peak centroid positions correspond to the vortex centres marked by red squares on the flow velocity field (Figure 22). The identified centres are also plotted together with the image velocity field in Figure 22: blue triangle for Δ-criterion, brown gradient for Q-criterion, pink diamond for circulation and black circle for vorticity.

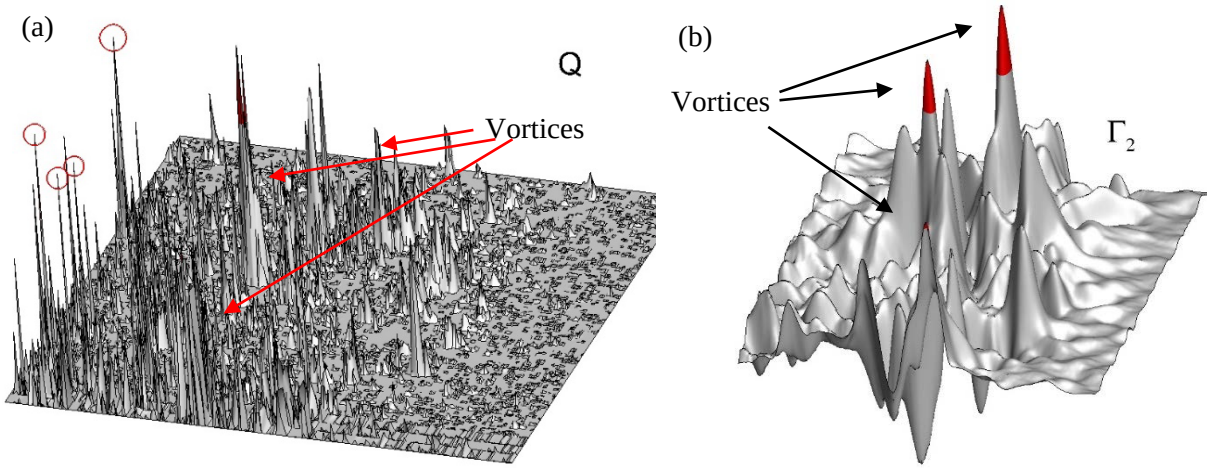

Figure 21. Turbulent flow: a) Q-criterion; b) Γ_2-criterion.

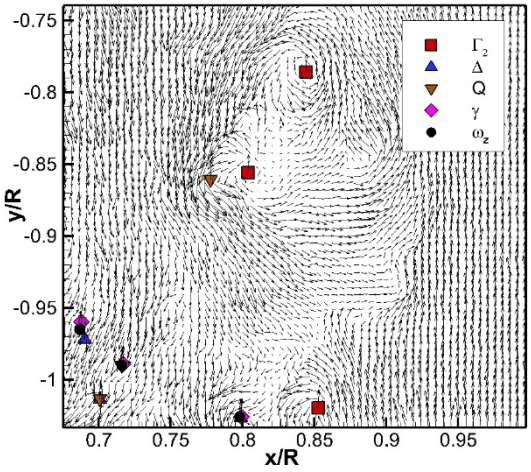

Figure 22. Flow velocity field in the wake turbulent region with the detected vortices.

The Γ_2 criterion shows better characteristics of robustness and reliability than the others do. Γ_2 is not affected by the blade passage at z/R=0, the centres are confined in the shear layer boundary with a uniform distribution and do not present the centres concentration on the left bottom corner outside the shear layer region. Moreover, in the wake region the presence of highly unsteady velocity fluctuations do not deteriorate the capability of Γ_2 method to identify vortices.

5 Conclusions

An effective criterion for detecting vortices within PIV data has been investigated. For this purpose, the Γ_2 method was selected and compared with some of the most popular vortex identification criteria. The different criteria were tested on special synthetic velocity fields as well as real PIV data. In order to assess the reliability of the Γ_2 criterion, a parametric analysis was carried out by using numerically-generated velocity fields containing a single (main) or a couple (main plus secondary) of theoretical vortices, co-rotating or counter rotating. The synthetic velocity fields presented different spatial resolution and noise levels to test the reliability of the vortex detection criteria.

The results showed a successful vortex detection for all the methods for the single vortex without noise, whereas only the Γ_2 criterion was able to confine the vortex region and identify the vortex centre with the increase in noise. Furthermore, the parametric study on the single vortex suggested the

appropriate value of the domain radius to be used. In the case of PIV data, the most effective domain radius turned out to be as close as possible to the value of the vortex core radius.

For synthetic multiple vortices, Γ_2 criterion is able to identify the vortex centres for all the velocity field without spurious vectors. The other criteria correctly detect the centre in case of multiple circular vortices, but in case of merging elliptical vortex or resulting velocity field with only a single vortex due to disappear of the other one, the criteria fails in detecting the vortices over estimating the number.

Adding white noise, the centres were detected by setting the domain radius as follow: equal to the major semi-axis dimension in case of elliptical vortex; equal to the radius size in case of equal contra-rotating vortices; like to the larger core radius in case of different vortices. The other criteria fail in detecting the vortices as the white noise percentage increase.

The Γ_2 criterion presented remarkable results in terms of robustness and reliability on the real PIV data, in particular for the case of the strong laser reflection in the measurement region. It can be then concluded that this criterion can be a valid alternative to complex algorithms for masking the images removing the laser reflection or to strong data filtering aimed at removing spurious vectors. Furthermore, the Γ_2 criterion has shown to be quite robust because the method does not require any fine tuning or the selection of threshold values for an optimization, once the radius of the domain has been selected.

References

[1] Raffel M, Bauknecht A, Ramasamy M, Yamauchi G, Heineck J T, Jenkins L N 2017 Contributions of Particle Image Velocimetry to Helicopter Aerodynamics, *AIAA Journal* 55 (3): 2859-2874
[2] De Gregorio F, Pengel K, Kindler K 2012 A comprehensive PIV Measurement Campaign on a Fully Equipped Helicopter Model *Experiments in Fluids* **53** (1) 37-49
[3] Lugt, H J 1983 Vortex flow in nature and technology (New York: Wiley & Sons)
[4] Robinson S K 1991 Coherent motion in turbulent boundary layer. *Annual Review of Fluid Mechanics*, **23** 601–639
[5] Chakraborty P, Balachandar S and Adrian R J 2005 On the relationships between local vortex identification schemes. *J. Fluid Mech.* **535** 189–214
[6] Kolar V 2007 Vortex identification: New requirements and limitation. *Journal of Heat and Fluid Flow* **28** 638-652
[7] Epps B P 2017 Review of vortex identification methods. *Proc. 55th AIAA Aerospace Sciences Meeting* (Grapevine, Texas)
[8] Hunt J C R, Wray A A and Moin P 1988 Eddies, stream, and convergence zones in turbulent flows. *Centre for Turbulence Research Report* CTR-S88:193–208
[9] Dallmann U 1983 Topological structures of three-dimensional flow separation *DFVLR-IB Report* No. 221-82 A07
[10] Vollmers H, Kreplin H P, Meier H U 1983 Separation and vertical type flow around a prolate spheroid – Evaluation of relevant parameters *AGARDCP-342* 14.1-14
[11] Chong M S 1990 A general classification of three-dimensional flow fields. *J. Phys. Fluids* **A2** 765-777
[12] Vollmers H 2001 Detection of vortices and quantitative evaluation of their main parameters from experimental velocity data. *Meas. Sci. Technol.* **12** 1199-1207
[13] Graftieaux L, Michard M and Grosjean N 2001 Combining PIV, POD and vortex identification algorithms for the study of unsteady turbulent swirling flows. *Meas. Sci. Technol.* **12**1422–1429
[14] Mulleners K and Raffel M 2011 The onset of dynamic stall revisited. *Exp. Fluids* **52** 779-793
[15] Michard M and Favelier T 2004 Développement d'un critère d'identification de structures tourbillonnaires adapté aux mesures de vitesse par PIV. *Proc. 9° Congrès Francophone de Vélocimétrie Laser* (Bruxelles)
[16] Vatistas G H 1998 New Model for Intense Self-Similar Vortices. *Journal of Propulsion and Power* **14** 462-469
[17] Scully M P 1975 Computation of Helicopter Rotor Wake Geometry and Its Influence on Rotor Harmonic Airloads *MIT Aeroelastic and Structures Research Laboratory*, ASRL TR 178-1

[18] Visingardi A, De Gregorio F, Schwarz T, Schmid M et al. 2017 Forces on Obstacles in Rotor Wake – A GARTEUR Action Group *Proc. 43rd European Rotorcraft Forum* (Milan, Italy)
[19] De Gregorio F, Visingardi A and Nargi R E 2018 Investigation of a Helicopter Model Rotor Wake interacting with a Cylindrical Sling Load. *Proc. 44th European Rotorcraft Forum* (Delft, The Netherlands)
[20] Martin P B, Pugliese G J, Leishman J G and Anderson S L 2000 Stereoscopic PIV measurement in the wake of a hovering rotor. *Proc. 56th American Helicopter Society Annual Forum* (Virginia Beach, VA)
[21] Mendez M A, Raiola M, Masullo A, Discetti S, Ianiro A, Theunissen R and Buchlin J M, 2017 POD-Based Background Removal for Particle Image Velocimetry, *Experimental Thermal and Fluid Science*, **80** 181–192